Eur. J. Mineral., 35, 635–643, 2023
https://doi.org/10.5194/ejm-35-635-2023

European Journal of Mineralogy
Open Access

Hochleitnerite, $[K(H_2O)]Mn_2(Ti_2Fe)(PO_4)_4O_2(H_2O)_{10} \cdot 4H_2O$, a new paulkerrite-group mineral, from the Hagendorf-Süd pegmatite, Oberpfalz, Bavaria, Germany

Ian E. Grey[1], Erich Keck[2], Anthony R. Kampf[3], Colin M. MacRae[1], Robert W. Gable[4], William G. Mumme[1], Nicholas C. Wilson[1], Alexander M. Glenn[1], and Cameron Davidson[1]

[1]CSIRO Mineral Resources, Private Bag 10, Clayton South, Victoria 3169, Australia
[2]private address: Algunderweg 3, 92694 Etzenricht, Germany
[3]Mineral Sciences Department, Natural History Museum of Los Angeles County, 900 Exposition Boulevard, Los Angeles, CA 90007, USA
[4]School of Chemistry, University of Melbourne, Parkville, Victoria 3010, Australia

Correspondence: Ian E. Grey (ian.grey@csiro.au)

Received: 27 June 2023 – Revised: 6 July 2023 – Accepted: 8 July 2023 – Published: 7 August 2023

Abstract. Hochleitnerite, $[K(H_2O)]Mn_2(Ti_2Fe)(PO_4)_4O_2(H_2O)_{10} \cdot 4H_2O$, is a new paulkerrite-group mineral from the Hagendorf-Süd pegmatite, Oberpfalz, Bavaria, Germany. It was found in specimens of altered zwieselite, in association with fluorapatite, rockbridgeite, columbite and sub-micrometre rods of uranophane. Hochleitnerite occurs as isolated and intergrown pale-yellow, diamond-shaped tablets with thicknesses reaching 50 µm and lengths of 120 µm. The crystals are flattened on {010}, slightly elongated on [001], and bounded by the {111} and {010} forms. The calculated density is 2.40 g cm^{-3}. Optically, hochleitnerite crystals are biaxial (+), with $\alpha = 1.615(2)$, $\beta = 1.621(2)$ and $\gamma = 1.645(2)$ (measured in white light). The calculated $2V$ is 53.8°. The empirical formula is $[K(H_2O)](Mn^{2+}_{1.51}Fe^{2+}_{0.49})_{\Sigma 2.00}(Ti^{4+}_{1.62}Fe^{3+}_{0.19}Al_{0.15})_{\Sigma 2.96}(PO_4)_{4.00}[O_{1.50}F_{0.23}(OH)_{0.27}]_{\Sigma 2.00}(H_2O)_{10} \cdot 4H_2O$. Hochleitnerite has space group *Pbca* and unit-cell parameters $a = 10.5513(3)$ Å, $b = 20.6855(17)$ Å, $c = 12.4575(4)$ Å, $V = 2718.96(15)$ Å^3 and $Z = 4$. The crystal structure was refined using single-crystal data to $wR_{obs} = 0.082$ for 2242 reflections with $I > 3\sigma(I)$. The crystal structure contains corner-connected linear trimers of Ti-centred octahedra that share corners with PO_4 tetrahedra to form 10-member rings parallel to (010). K^+ cations and water molecules are located within the rings. Additional corner sharing of the PO_4 tetrahedra with $MnO_2(H_2O)_4$ octahedra occurs along [010] to complete the 3D framework structure.

1 Introduction

Hochleitnerite was found by one of the authors (Erich Keck) in specimens of altered zweiselite that he collected in the 1970s at the 64 to 76 m level of the Hagendorf Süd pegmatite mine in the Oberpfalz, northeastern Bavaria, Germany (49°39′1″ N, 12°27′35″ E). It was identified by Erich Keck as a benyacarite-related mineral (Keck et al., 1998), and the specimen was forwarded in 2019 to CSIRO, Melbourne, for further characterisation as part of an ongoing Australian–Bavarian collaborative study on secondary phosphate minerals from the now defunct Hagendorf Süd pegmatite mine (Birch et al., 2018). Single-crystal diffraction studies combined with electron microprobe (EMP) analyses confirmed the mineral to be a new species, which was approved by the International Mineralogical Association (IMA) Commission on New Minerals, Nomenclature and Classification (CNMNC), IMA-2022-141.

The name honours Rupert Hochleitner (born 1954) for his important contributions to the crystal chemistry of min-

erals and the dissemination of knowledge on mineral identification through his books on the subject, translated into 12 languages. After completion of his doctoral thesis at the Institute of Crystallography and Applied Mineralogy, Ludwig Maximilian University, Munich, Rupert Hochleitner was chief editor of the mineralogical journal *Lapis* for 14 years. In 1993 he became vice director of the Mineralogical State Collection, Munich (SNSB), where he worked until his retirement in 2019. He is currently an honorary scientist at the Mineralogical State Collection. Rupert Hochleitner has published extensively on the application of Mössbauer, Raman and NMR spectroscopy to mineral characterisation. He has made major contributions to publications describing the characterisation of the Hagendorf Süd minerals keckite, Mn-bearing eleonorite, whiteite-(CaMnFe) and pleysteinite. Rupert Hochleitner has given his permission for the mineral name. The holotype specimen is housed in the mineralogical collections of the Natural History Museum of Los Angeles County, catalogue number 76 277. The Dana classification number for hochleitnerite is 43.11.21 (Gaines et al., 1997), defined as the paulkerrite group, which includes paulkerrite (Peacor et al., 1984), mantiennéite (Fransolet et al., 1984) and benyacarite (Demartin et al., 1993, 1997). The paulkerrite group has been approved by the IMA CNMNC, proposal 22-K-bis, with the addition of new members pleysteinite (Grey et al., 2023), hochleitnerite and rewitzerite (IMA 2023-005).

2 Occurrence and paragenesis

Hochleitnerite crystals occur on altered zwieselite (Fig. 1). The zwieselite, with composition $Fe_{1.2}Mn_{0.8}(PO_4)F$, is bleached to a pale-yellow colour and is microporous. Minerals closely associated with hochleitnerite and zwieselite are rockbridgeite, fluorapatite, columbite and sub-micrometre rods of uranophane. Other associated minerals are quartz and a jahnsite-group mineral.

Titanium-bearing minerals are very rare at Hagendorf Süd, with only biotite, ilmenite and a variety of uranpyrochlore recorded in Mindat. The most likely source of the Ti in hochleitnerite is the altered zwieselite matrix that it is in contact with. Chemical analyses of zwieselite in altered zwieselite specimens from five different locations at the Hagendorf pegmatite give TiO_2 contents in the range 0.08 wt % to 0.19 wt %. The presence of hochleitnerite crystals lining vugs formed by leaching of zwieselite suggests that hochleitnerite formed from zwieselite by dissolution–reprecipitation, and the presence of considerable H_2O in its formula indicates that this occurred at a relatively low temperature.

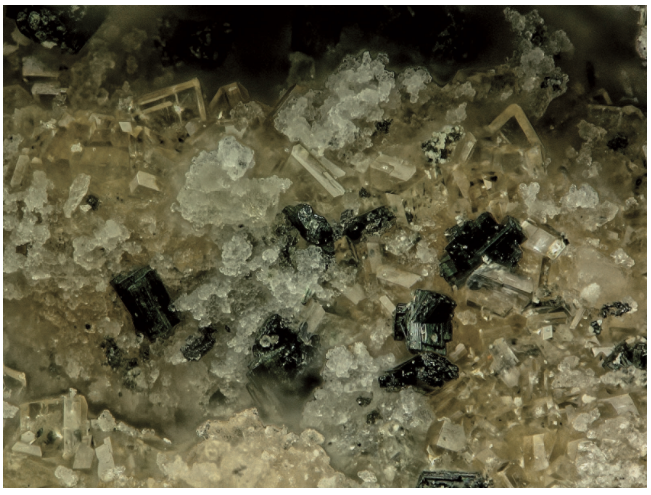

Figure 1. Transparent crystals of hochleitnerite associated with colourless microcrystalline fluorapatite and black crystals of rockbridgeite. Field of view: 0.84 mm. Photo by Anthony Kampf.

3 Physical and optical properties

Hochleitnerite forms isolated and intergrown pale-yellow, diamond-shaped tablets on fine-grained zwieselite (Figs. 1 and 2). The crystals have dimensions of typically 20 to 80 µm. The crystals are flattened on {010}, slightly elongated on [001], and bounded by the {111} and {010} forms (Fig. 3). The calculated density, for the empirical formula and single-crystal cell volume, is 2.40 g cm^{-3}.

Optically, hochleitnerite crystals are biaxial (+), with $\alpha = 1.615(2)$, $\beta = 1.621(2)$ and $\gamma = 1.645(2)$ (measured in white light). The calculated $2V$ is 53.8°; $2V$ could not be measured because of the presence of apparent sector zoning, which distorts the conoscopic figure and makes extinction observations unreliable. Dispersion was moderate with $r < v$, and pleochroism was not observed. The optical orientation is $X = \boldsymbol{b}$, $Y = \boldsymbol{c}$ and $Z = \boldsymbol{a}$. The Gladstone–Dale compatibility index (Mandarino, 1981) is 0.027 (excellent) based on the empirical formula and the calculated density.

4 Chemical composition

Crystals of hochleitnerite were analysed using wavelength-dispersive spectrometry on a JEOL JXA 8500F Hyperprobe operated at an accelerating voltage of 15 kV and a beam current of 2.2 nA. The beam was defocused to 10 µm. Analytical electron microprobe (EMP) results (average of 12 analyses on 12 different crystals) are given in Table 1. There was insufficient material for direct determination of H_2O, the presence of which was indicated by the low EMP analysis sum of oxides and confirmed by Raman spectroscopy, so it was based upon the crystal structure analysis with 15 H_2O per formula unit. The Fe^{2+} / Fe^{3+} ratio was based on the crystal

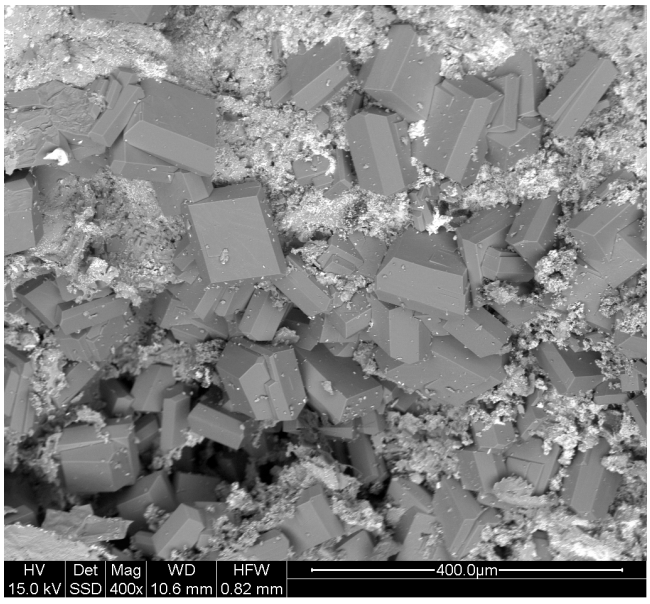

Figure 2. Back-scattered electron image of hochleitnerite crystals on zwieselite.

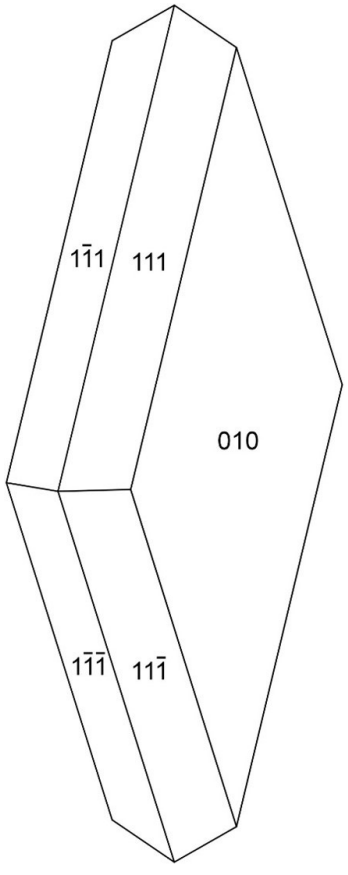

Figure 3. Crystal drawing of hochleitnerite and clinographic projection in standard orientation.

Table 1. Analytical data (wt%) for hochleitnerite.

Constituent	Mean	Range	SD	Standard
K_2O	4.64	4.35–5.23	0.32	Adularia
MnO	10.65	9.56–11.69	0.68	$MnSiO_3$
MgO	0.04	0.00–0.14	0.08	Spinel
Al_2O_3	0.64	0.17–1.24	0.32	Berlinite
Fe_2O_3 (total)	(13.52)	12.75–14.21	0.53	Hematite
FeO*	3.36			
$Fe_2O_3^*$	9.78			
TiO_2	12.95	11.55–14.04	0.83	Rutile
P_2O_5	28.08	25.41–31.64	1.73	Berlinite
F	0.44	0.10–0.99	0.26	Fluorite
H_2O_{calc}	26.87			
$-O \equiv F$	−0.19			
Total	97.27			

* Fe^{2+} / Fe^{3+} based on the crystal structure, with Fe^{2+} assigned with all Mn^{2+} and Mg at the $M1$ site and the remaining iron as Fe^{3+} assigned to the $M2$ and $M3$ sites.

structure, with Fe^{2+} assigned with all other divalent elements (Mg and Mn^{2+}) to the $M1$ site, and the remaining iron as Fe^{3+} was assigned to the $M2$ and $M3$ sites.

The EMP results were normalised to 9 cations per formula unit and 33 (O + F), giving the atomic fractions $K_{1.00}Mn_{1.51}Fe^{2+}_{0.49}Fe^{3+}_{1.19}Ti_{1.62}Al_{0.15}P_{4.00}O_{32.77}F_{0.23}H_{30.27}$. The least-squares program OccQP (Wright et al., 2000) was used to optimise the site occupations for the $M1$ to $M3$ sites based on the refined site scattering and bond lengths from the crystal structure refinement combined with the chemical analyses, giving the following structural formula: $^{A}[(H_2O)_{1.00}K_{1.00}]_{\Sigma 2.00}$ $^{M1}(Mn^{2+}_{1.51}Fe^{2+}_{0.49})_{\Sigma 2.00}$ $^{M2}(Ti^{4+}_{1.08}Fe^{3+}_{0.73}Al_{0.15})_{\Sigma 1.96}$ $^{M3}(Ti^{4+}_{0.54}Fe^{3+}_{0.46})_{\Sigma 1.00}(PO_4)_{4.00}[O_{1.50}F_{0.23}(OH)_{0.27}]_{\Sigma 2.00}(H_2O)_{10} \cdot 4H_2O$. The corresponding end-member formula is $[H_2O]_2Mn_2Ti_3(PO_4)_4O_2(H_2O)_{10} \cdot 4H_2O$.

Although this formula was approved by the IMA CNMNC (IMA-2022-141), it was criticised by some voting members because it does not include K, which is co-dominant with H_2O at the A site. The problem arises because of almost complete mixing of Ti and Fe^{3+} at the crystalochemically similar $M2$ and $M3$ sites, so the constituent assignments at these two sites depend sensitively on the location of the minor Al. With Al located at the $M3$ site rather than at the $M2$ site, the program OccQP gives dominant Fe^{3+}, rather than Ti at the $M3$ site, and leads to the alternative end-member formula $[K(H_2O)]Mn_2Ti_2Fe(PO_4)_4O_2(H_2O)_{10} \cdot 4H_2O$. To overcome the problem, common in paulkerrite group minerals, of very strong mixing of Fe^{3+} and Ti at the $M2$ and $M3$ sites, the compositions of these two sites were merged. The resulting empirical chemical formula can hence be rewritten as $^{A}[(H_2O)_{1.00}K_{1.00}]_{\Sigma 2.00}$ $^{M1}(Mn^{2+}_{1.51}Fe^{2+}_{0.49})_{\Sigma 2.00}$ $^{M2+M3}(Ti^{4+}_{1.62}Fe^{3+}_{1.19}\ Al_{0.15})_{\Sigma 2.96}(PO_4)_{4.00}$ $[O_{1.50}F_{0.23}(OH)_{0.27}]_{\Sigma 2.00}(H_2O)_{10} \cdot 4H_2O$.

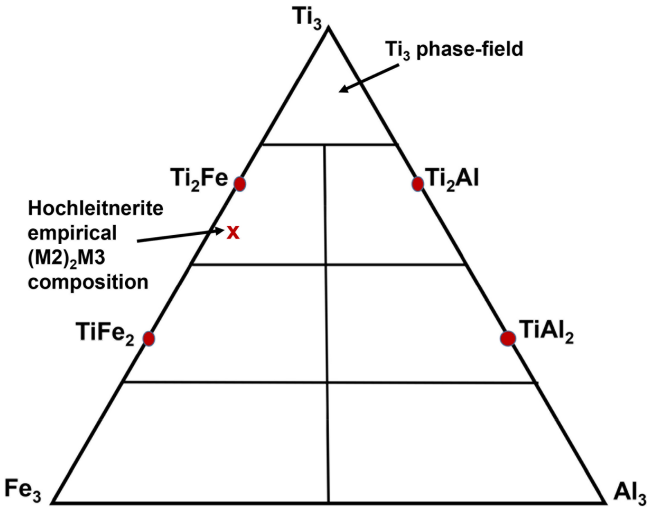

Figure 4. Ternary diagram for $(M2)_2M3$ site Al–Ti–Fe^{3+} compositions, showing end-member compositions (Al_2Ti, $AlTi_2$, etc.) and the location of the experimental composition of hochleitnerite.

This formula disregards the Ti–Fe^{3+} disordering over $M2$ and $M3$ and leads to the end-member formula $[K(H_2O)]Mn_2(Ti_2Fe)(PO_4)_4O_2(H_2O)_{10} \cdot 4H_2O$, which requires K_2O 4.79, MnO 14.44, Fe_2O_3 8.13, TiO_2 16.26, P_2O_5 28.90 and H_2O 27.448, with a total of 100.00 wt %. This revised formula was approved by the IMA-CNMNC in a paulkerrite-group mineral nomenclature proposal (revised proposal 22-K-bis). The details of this nomenclature, based on site-total-charge method (Bosi et al., 2019), will be reported separately, but the result for the merged $M2$ and $M3$ site compositions is illustrated by the ternary diagram shown in Fig. 4. This diagram shows the possible end-member compositions based on the occupation of $(M2)_2M3$ by Al, Ti and Fe^{3+}. The empirical composition of hochleitnerite, shown by the cross, is located in the compositional field for the end-member (Ti_2Fe).

5 Raman spectroscopy

Raman spectroscopy was conducted on a Horiba XploRA PLUS spectrometer using a 532 nm diode laser, 100 µm slit, 1800 g mm^{-1} diffraction grating and a 100× (0.9 NA) objective. The spectrum is shown in Fig. 5. The O–H stretching region has a broad peak with maxima at 3470, 3225, and 3305 cm^{-1} and a sharp shoulder at 3580 cm^{-1}. The H–O–H bending mode region for water has a peak at 1660 cm^{-1}. The P–O stretching region has three peaks at 955, 975 and 1015 cm^{-1} and two weaker peaks at 1080 and 1130 cm^{-1}. The three stronger peaks correspond to symmetric stretching modes, and the weaker peaks correspond to symmetric P–O stretching modes. Bending modes of the $(PO_4)^{3-}$ groups are manifested by a band centred at 590 cm^{-1} and a pair of bands at 440 and 470 cm^{-1}. Peaks at lower wavenumbers are

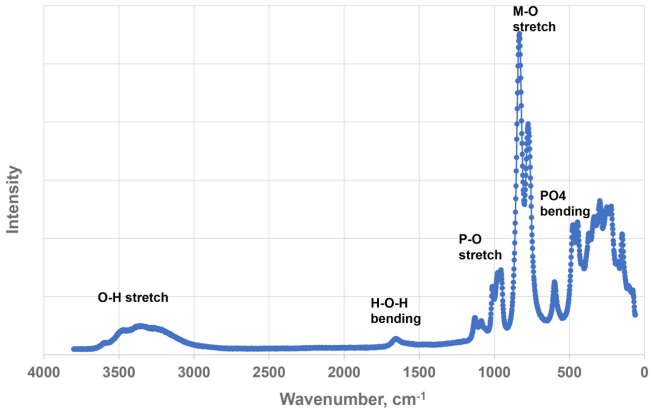

Figure 5. Raman spectrum for hochleitnerite.

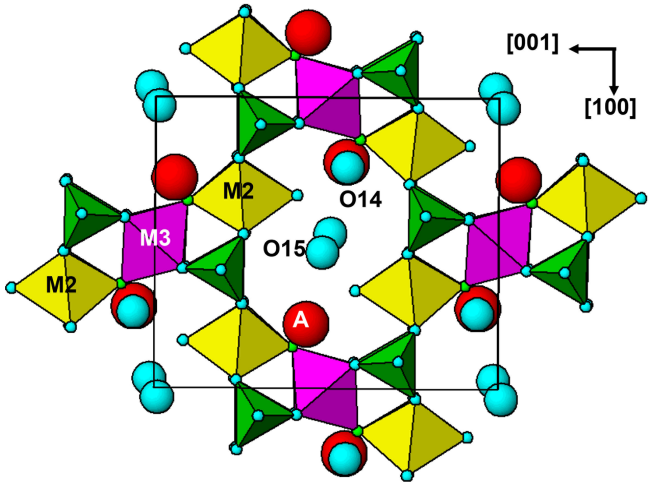

Figure 6. The (010) slice of the hochleitnerite structure.

related to lattice vibrations. The intense pair of peaks at 775 and 850 cm^{-1} is an interesting feature of the spectrum. The tentative assignment of the peaks is to M–(O,F) stretching vibrations for short M–X bonds that occur in linear trimers of corner-connected octahedra $M2$–$M3$–$M2$ in the structure, where X is the bridging anion between the octahedra (Fig. 6). The potassium titanyl phosphate, $KTiOPO_4$, has chains of corner-connected octahedra with alternating short and long Ti–O bonds, and the Raman spectrum has an intense band at 770 cm^{-1} that has been assigned to the symmetric Ti–O stretching vibration (Tu et al., 1996). Strong Raman bands in the range 800 to 900 cm^{-1} have been reported and assigned to Ti–O stretch vibrations for several potassium titanium oxides, which have corner-connected TiO_6 octahedra involving short (∼ 1.8 Å) Ti–O bonds (Bamberger et al., 1990). The $M2$ site in hochleitnerite similarly has the $M2$ atom displaced from the centre of the octahedron towards the corner-sharing X anion with the $M3$-centred octahedron giving a short (1.806 Å) $M2$–(O,F) bond.

6 Crystallography

X-ray powder diffraction data were recorded using a Rigaku *R*-Axis Rapid II curved imaging plate microdiffractometer with monochromatised Mo$K\alpha$ radiation. A Gandolfi-like motion on the ϕ and ω axes was used to randomise the sample. Observed d values and intensities were derived by profile fitting using JADE Pro software (Materials Data, Inc.). Data are given in Table 2. Refined orthorhombic unit-cell parameters (space group *Pbca* (#61)) are $a = 10.557(10)$ Å, $b = 20.710(18)$ Å, $c = 12.502(11)$ Å, $V = 2733.3(2)$ Å^3 and $Z = 4$.

Single-crystal data were collected at 294 K using a XtaLAB Synergy four-circle diffractometer equipped with a Dualflex Hypix detector and using Mo$K\alpha$ radiation, $\lambda = 0.71073$ Å. Refined unit-cell parameters and other data collection details are given in Table 3.

Structure refinement

A structural model for hochleitnerite was obtained in space group *Pbca* using SHELXT (Sheldrick, 2015). It was found to be the same as that reported for benyacarite, $(H_2O,K)_2M1_2M2_2Ti(PO_4)_4(O,F)_2 \cdot 14H_2O$ (Demartin et al., 1993), where the $M1$ and $M2$ sites contain divalent and trivalent cations, respectively. Based on bond lengths, Mn^{2+} from the EMP analysis was assigned to the $M1$ site with Fe^{2+} completing the site filling. The scattering curves for Fe and Ti were used for the $M2$ and $M3$ sites, respectively, and a mix of K and O (for H_2O) was assigned to the A site. Refined site scattering values were used in the program OccQP to optimise site populations.

Refinement with anisotropic displacement parameters for all atoms in JANA2006 (Petříček et al., 2014) converged at $R_{obs} = 0.065$ for 2242 reflections with $I > 3\sigma(I)$. An unambiguous location of H atoms in the correct configurations for H_2O molecules in difference Fourier maps was not achieved. Partial H positions have been previously reported for benyacarite (Demartin et al., 1993). Details of the data collection and refinement are given in Table 3. It is interesting to note that although the merging R_{int} factor was high (20 %) due to weak reflection intensities (mean $I/\sigma(I) = 2.9$), the high redundancy in measured reflections of 10.3 resulted in averaged intensities that led to a reasonable refinement and sensible crystal chemistry of the model.

The refined coordinates, equivalent isotropic displacement parameters and bond valence sum (BVS) values (Gagné and Hawthorne, 2015) from the single-crystal refinement are reported in Table 4. Selected interatomic distances are reported in Table 5. Although the H atoms were not located, the BVS values in Table 4 clearly show the presence of seven independent H_2O groups, O9 to O15.

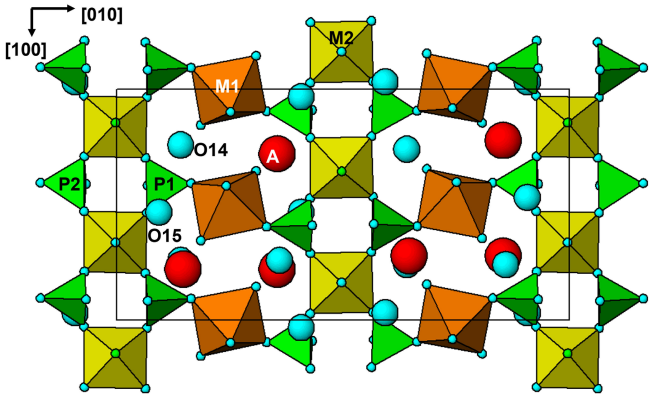

Figure 7. The (001) slice through the structure of hochleitnerite.

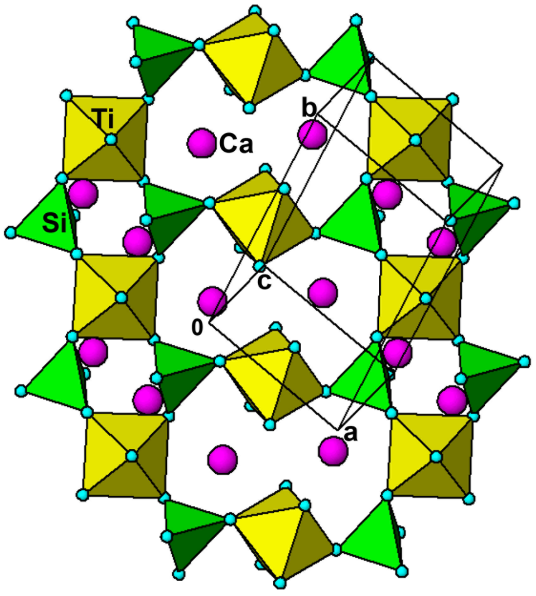

Figure 8. The (11-2) layer in the crystal structure for titanite, showing same heteropolyhedral topology as for the (001) layer in hochleitnerite (Fig. 7).

7 Discussion

Hochleitnerite is isostructural with benyacarite (Demartin et al., 1993, 1997) and the recently described Al analogue pleysteinite (Grey et al., 2023). A key feature of the structure is the presence of linear trimers of corner-connected octahedra $M2$–$M3$–$M2$, which are oriented approximately parallel to [102] and [−102] as shown in Fig. 6. The $M2$- and $M3$-centred octahedra have compositions $M2O_4X(H_2O)$ and $M3O_4X_2$, respectively, where O anions are shared with PO_4 tetrahedra and X is the bridging anion between the octahedra. The $M2$-centred octahedron is characterised by a displacement of $M2$ towards X to give a short $M2$–X distance of 1.80 Å and a much longer opposing $M2$–H_2O distance of 2.16Å. The octahedral distortion is similar to that occurring

Table 2. Powder X-ray diffraction data (d in Å) for hochleitnerite (I_{calc}>2.5). Strongest reflections shown in bold.

I_{obs}	d_{obs}	d_{calc}	I_{calc}	hkl	I_{obs}	d_{obs}	d_{calc}	I_{calc}	hkl
51	**10.32**	10.3428	59	0 2 0	13	2.335	2.3292	9	1 8 2
55	**7.51**	7.5031	73	1 1 1	8	2.201	2.1985	5	4 4 2
72	**6.24**	6.2288	100	0 0 2			2.1896	3	4 5 1
43	**5.23**	5.2757	21	2 0 0	6	2.128	2.1415	3	2 3 5
		5.2371	11	1 3 1			2.0950	3	4 6 0
		5.1714	15	0 4 0	11	2.086	2.0763	11	0 0 6
10	4.73	4.6996	6	2 2 0	4	2.013	2.0129	5	4 0 4
		4.0257	6	2 0 2	29	1.9867	1.9857	21	4 6 2
33	3.988	3.9713	28	2 3 1			1.9757	5	3 8 2
		3.7983	3	1 1 3			1.9624	3	5 2 2
52	**3.747**	3.7515	49	2 2 2			1.9438	3	4 7 1
		3.6930	8	2 4 0	12	1.9296	1.9314	3	3 6 4
4	3.425	3.4476	3	0 6 0			1.9268	5	0 4 6
		3.3708	4	1 3 3	6	1.8975	1.8992	10	2 2 6
		3.1767	4	2 4 2	9	1.8712	1.8735	10	5 1 3
100	**3.141**	3.1497	54	2 5 1			1.8615	4	2 8 4
		3.1144	26	0 0 4	12	1.8388	1.8399	7	2 10 2
		3.0626	10	3 0 2	11	1.7920	1.7880	8	3 0 6
		3.0384	3	3 3 1			1.7783	4	4 7 3
39	3.013	3.0164	10	0 6 2			1.7383	4	4 6 4
		2.9870	17	1 0 4	16	1.7297	1.7238	10	0 12 0
		2.9494	5	2 3 3			1.7163	3	4 9 1
		2.9366	3	3 2 2			1.7012	3	5 7 1
59	**2.881**	2.8860	28	2 6 0	17	1.6911	1.6898	4	3 4 6
		2.8697	10	1 2 4			1.6854	7	2 6 6
10	2.822	2.8239	14	1 5 3	10	1.6693	1.6649	12	6 4 0
		2.6819	6	2 0 4			1.6613	4	0 12 2
		2.6679	4	0 4 4			1.6385	4	2 12 0
60	**2.619**	2.6352	15	3 4 2	31	1.6201	1.6277	3	4 10 0
		2.6186	15	2 6 2			1.6116	7	4 2 6
		2.5865	9	1 4 4			1.6085	4	6 4 2
8	2.553	2.5608	14	4 1 1	8	1.5701	1.5749	6	4 10 2
16	2.519	2.5247	13	2 7 1			1.5681	4	5 3 5
		2.5010	7	3 3 3					
6	2.383	2.3808	3	2 4 4					
		2.3647	6	4 2 2					

in compounds containing the titanyl ion such as $KTiO(PO_4)$ and gives rise to a strong Raman band near 800 cm^{-1} as discussed in the Raman spectroscopy section. Such a distortion is not possible for the $M3$-centred octahedron, since it is located at an inversion centre and has three pairs of equivalent anions, but the two $M3$–X distances are considerably shorter than the four $M3$–O distances. The octahedral trimers are interconnected via corner sharing with PO_4 tetrahedra to form (010) heteropolyhedral layers shown in Fig. 6. The corner-connected octahedra and tetrahedra form 10-member rings that border cavities containing the A-site species (K^+ and H_2O) and water molecules (O14 and O15 in Table 4). The water molecule O15 is coordinated to K at the A site at a distance of 2.88 Å, while O14 only has H-bonded contacts.

The (010) heteropolyhedral layers are interconnected along [010] into a 3D framework via $M1$-centred octahedra

Table 3. Crystal data and structure refinement for hochleitnerite.

End-member formula	$[K(H_2O)]Mn_2(Ti_2Fe)(PO_4)_4O_2(H_2O)_{10} \cdot 4H_2O$
Formula weight	953.46
Temperature	294 K
Wavelength	0.71073 Å
Space group	*Pbca* (#61)
Unit cell dimensions	$a = 10.5513(3)$ Å
	$b = 20.6855(7)$ Å
	$c = 12.4575(4)$ Å
Volume	2718.96(15) Å^3
Z	4
Absorption correction	Gaussian, $\mu = 2.46\,\mathrm{mm}^{-1}$
Crystal size	$0.09 \times 0.10 \times 0.13$ mm
Theta range for data collection	2.56 to 31.95°
Index ranges	$-15 \le h \le 14$, $-28 \le k \le 30$, $-18 \le l \le 17$
Reflections collected	44 079
Independent reflections	4268
Reflections with $I_o > 3\sigma(I)$	2242
Refinement method	Full-matrix least-squares on F
Data/restraints/parameters	4268/0/190
Final R indices $[I > 3\sigma(I)]$	$R_{obs} = 0.065$, $wR_{obs} = 0.082$
R indices (all data)	$R_{obs} = 0.128$, $wR_{obs} = 0.087$
Largest diff. peak and hole	1.61 and $-1.14\,e$ Å^{-3}

Table 4. Atom coordinates, equivalent isotropic displacement parameters (Å^2) and bond valence sums (BVS, in valence units) for hochleitnerite.

	x	y	z	U_{eq}	BVS
$M1$	0.49545(7)	0.74635(4)	0.24253(6)	0.0204(2)	2.07
$M2$	0.66195(7)	0.50315(4)	0.74050(6)	0.0150(2)	3.56
$M3$	0.5	0.5	0.5	0.0173(3)	3.57
P1	0.90924(11)	0.59589(7)	0.80236(9)	0.0143(4)	5.03
P2	0.58472(12)	0.59052(7)	0.29554(9)	0.0147(4)	5.02
A	0.7211(2)	0.85380(12)	0.05789(17)	0.0368(8)	0.74
X^*	0.6448(3)	0.50309(18)	0.5963(2)	0.0167(10)	1.64
O1	0.9038(3)	0.66893(19)	0.8065(3)	0.0227(11)	1.76
O2	1.0280(3)	0.57292(18)	0.7414(3)	0.0202(10)	1.74
O3	0.9092(3)	0.56863(18)	0.9177(3)	0.0197(11)	1.80
O4	0.7899(3)	0.57181(18)	0.7444(3)	0.0198(11)	1.92
O5	0.5925(3)	0.66380(19)	0.2873(3)	0.0250(12)	1.75
O6	0.4654(3)	0.56571(18)	0.2374(3)	0.0197(10)	1.82
O7	0.5829(3)	0.56849(18)	0.4128(3)	0.0195(11)	1.90
O8	0.7043(3)	0.56289(18)	0.2410(3)	0.0224(11)	1.83
O9	0.3442(3)	0.6848(2)	0.1756(3)	0.0331(14)	0.34
O10	0.5823(3)	0.7414(2)	0.0765(3)	0.0308(13)	0.34
O11	0.6454(3)	0.8080(2)	0.3100(3)	0.0343(14)	0.34
O12	0.4013(4)	0.7508(2)	0.4043(3)	0.0335(13)	0.34
O13	0.6631(3)	0.5029(2)	0.9141(3)	0.0273(12)	0.35
O14	0.2596(4)	0.6403(2)	0.4409(3)	0.0368(15)	0.0
O15	0.5326(5)	0.4071(3)	1.0114(3)	0.057(2)	0.05

Site scattering (electrons): $M1 = 25.25$; $M2 = 22.34$; $M3 = 23.84$. A site occupancy $= K_{0.438(9)}O_{0.562(9)}$. X^* denotes the bridging anion site between $M2$- and $M3$-centred octahedra.

Table 5. Polyhedral bond lengths [Å] for hochleitnerite.

P1–O1	1.513(4)	P2–O5	1.521(4)
P1–O2	1.541(4)	P2–O6	1.541(4)
P1–O3	1.543(3)	P2–O7	1.530(3)
P1–O4	1.534(4)	P2–O8	1.543(4)
avg	1.533	avg	1.534
*M*1–O1	2.093(4)	A–*X*	3.105(4)
*M*1–O5	2.068(4)	A–O4	2.880(4)
*M*1–O9	2.205(4)	A–O7	2.824(4)
*M*1–O10	2.264(4)	A–O10	2.758(5)
*M*1–O11	2.198(4)	A–O12	2.895(5)
*M*1–O12	2.249(4)	A–O15	2.882(6)
avg	2.180	avg	2.891
*M*2–*X*	1.806(3)	*M*3–*X* (×2)	1.943(3)
*M*2–O2	2.032(4)	*M*3–O3 (×2)	1.996(4)
*M*2–O4	1.961(4)	*M*3–O7 (×2)	1.988(3)
*M*2–O6	1.978(4)	avg	1.976
*M*2–O8	1.964(4)		
*M*2–O13	2.163(3)		
avg	1.984		

of composition $M1O_2(H_2O)_4$. These octahedra share *trans* O anions with PO_4 tetrahedra as shown in Fig. 7. This view of the structure, an (001) slice, shows that the *M*2-centred octahedra and PO_4 tetrahedra form $M2(PO_4)_2X(H_2O)$ kröhnkite-type ribbons (Hawthorne, 1985) along [100]. The ribbon repeat distance along [100] of 10.55 Å in hochleitnerite is double that in kröhnkite due to the tetrahedra in successive four-member rings having their apices pointing in opposite directions along [001]. It is interesting to note that the heteropolyhedral layer in Fig. 7, containing four-member and eight-member rings, has topological equivalents in $GeOHPO_4$-type structures that include minerals such as kieserite ($MgSO_4 \cdot H_2O$), titanite ($CaTiOSiO_4$), lazulite ($MgAl_2(PO_4)_2(OH)_2$) and amblygonite ((Li,Na)Al(PO_4)(F,OH)) (Mayer and Völlenkle, 1972). The example of titanite is shown in Fig. 8 where the close heteropolyhedral layer relationship with hochleitnerite extends also to the Ca atoms, which occupy similar positions in the eight-member rings to the *A*-site cations in hochleitnerite. Other minerals that have the same topology of kröhnkite-type ribbons bridged by $MO_2(H_2O)_4$ octahedra as occurs in hochleitnerite (Fig. 7) include laueite-group minerals and geometrical isomers like stewartite (Krivovichev, 2004).

Data availability. Crystallographic data for Hochleitnerite are available in the Supplement.

Supplement. The supplement related to this article is available online at: https://doi.org/10.5194/ejm-35-635-2023-supplement.

Author contributions. IEG oversaw the research and wrote the paper. EK carried out the field collection of the specimen. ARK measured the optical properties, Raman spectrum PXRD and crystal morphology. CMM conducted the EMP analyses. RWG collected the single-crystal diffraction data. WGM assisted in the diffraction data analysis. NCW performed the site-assignment calculations using the program OccQP. AMG obtained energy-dispersive analyses and Fig. 2 from SEM studies. CD prepared polished mounts of the specimen for EMP analyses.

Competing interests. The contact author has declared that none of the authors has any competing interests.

Disclaimer. Publisher's note: Copernicus Publications remains neutral with regard to jurisdictional claims in published maps and institutional affiliations.

Acknowledgements. Special thanks go to Ferdinando Bosi for suggesting the site-total-charge method be applied to merged *M*2 and *M*3 sites to obtain the end-member formula. We thank Rupert Hochleitner for providing X-ray fluorescent analyses of altered zwieselite specimens from the Hagendorf pegmatite.

Review statement. This paper was edited by Sergey Krivovichev and reviewed by two anonymous referees.

References

Bamberger, C. E., Begun, G. M., and MacDougall, C. S.: Raman spectroscopy of potassium titanates: Their synthesis, hydrolytic reactions and thermal stability, Appl. Spectr., 44, 31–37, 1990.

Birch, W. D., Grey, I. E., Keck, E., Mills, S. J., and Mumme, W. G.: The Hagendorf Süd pegmatite: Australian-Bavarian collaboration on the characterisation of new secondary phosphate minerals, Aust. J. Mineral., 19, 7–19, 2018.

Bosi, F., Hatert, F., Halenius, U., Pasero, M., Ritsuro, M., and Mills, S. J.: On the application of the IMA-CNMNC dominant-valency rule to complex mineral compositions, Mineral. Mag., 83, 627–632, 2019.

Demartin, F., Pilati, T., Gay, H. D., and Gramaccioli, C. M.: The crystal structure of a mineral related to paulkerrite, Z. Kristallogr., 208, 57–71, 1993.

Demartin, F., Gay, H. D. Gramaccioli, C. M., and Pilati, T.: Benyacarite, a new titanium-bearing phosphate mineral species from Cerro Blanco, Argentina, Can. Mineral., 35, 707–712, 1997.

Fransolet, A.-M., Oustriere, P., Fontan, F., and Pillard, F.: La mantiennéite, une novelle espèce minérale du gisement de vivianite d'Anloua, Cameroun. Bull. Mineral., 107, 737–744, 1984.

Gagné, O. C. and Hawthorne, F. C.: Comprehensive derivation of bond-valence parameters for ion pairs involving oxygen, Acta Crystallogr., B71, 562–578, 2015.

Gaines, R. V., Skinner, C. W., Foord, E. E., Mason, B., and Rosenzweig, A.: Dana's New Mineralogy – The system of mineralogy

of James Dwight Dana and Edward Salisbury Dana, 8th Edn., John Wiley and Sons, New York, ISBN 9780471193104, 1997.

Grey, I. E., Hochleitner, R., Rewitzer, C., Kampf, A. R., MacRae, C. M., Gable, R. W., Mumme, W. G., Keck, E., and Davidson, C.: Pleysteinite, $[(H_2O)_{0.5}K_{0.5}]_2Mn_2Al_3(PO_4)_4F_2(H_2O)_{10} \cdot 4H_2O$, the Al analogue of benyacarite, from the Hagendorf-Süd pegmatite, Oberpfalz, Bavaria, Germany, Eur. J. Mineral., 35, 189–197, https://doi.org/10.5194/ejm-35-189-2023, 2023.

Hawthorne, F. C.: Towards a structural classification of minerals: The viMivT2Φn minerals, Am. Mineral., 70, 455–473, 1985.

Keck, E., Witzke, T., Pollmann, H., and Friese, K.: Benyacarit aus ostbayrischen und portugiesichen Pegmatiten, Aufschluss, 49, 281–285, 1998.

Krivovichev, S. V.: Topological and geometrical isomerism in minerals and inorganic compounds with laueite-type heteropolyhedral sheets, Neues Jb. Miner. Mh., 2004, 209–220, 2004.

Mandarino, J. A.: The Gladstone-Dale relationship: Part IV. The compatibility concept and its application, Can. Mineral., 19, 441–450, 1981.

Mayer, H. and Völlenkle, H.: Die Kristallstruktur und Fehlordnung von Ge(OH)P04, Z. Kristallogr., 136, 387–401, 1972.

Peacor, D. R., Dunn, P. J., and Simmons, W. B.: Paulkerrite a new titanium phosphate from Arizona, Mineral. Rec., 15, 303–306, 1984.

Petříček, V., Dušek, M., and Palatinus, L.: Crystallographic Computing System JANA2006: General features, Z. Krist., 229, 345–352, 2014.

Sheldrick, G. M.: Crystal-structure refinement with SHELX, Acta Crystallogr., C71, 3–8, 2015.

Tu, C.-S., Guo, A. R., Tao, R., Katiyar, R. S., Guo, R., and Bhalla, A. S.: Temperature dependent Raman scattering in $KTiOPO_4$ and $KTiOAsO_4$ single crystals, J. Appl. Phys., 79, 3235–3240, 1996.

Wright, S. E., Foley, J. A., and Hughes, J. M.: Optimisation of site occupancies in minerals using quadratic programming, Am. Mineral., 85, 524–531, 2000.